

# Parachute systems for the atmospheric reentry of launcher upper stages

Bogdan DOBRESCU\*<sup>1</sup>, Radu BLIDERAN<sup>1</sup>, Adrian CHELARU<sup>1</sup>

\*Corresponding author

<sup>1</sup>INCAS – National Institute for Aerospace Research “Elie Carafoli”,  
B-dul Iuliu Maniu 220, Sector 6, Bucharest 061126, Romania,  
dobrescu.bogdan@incas.ro\*, blideran.radu@incas.ro, chelaru.adrian@incas.ro

DOI: 10.13111/2066-8201.2017.9.1.4

Received: 16 November 2016/ Accepted: 03 December 2016/ Published: March 2017

© Copyright 2017, INCAS. This is an open access article under the CC BY-NC-ND license (<http://creativecommons.org/licenses/by-nc-nd/4.0/>)

*International Conference of Aerospace Sciences “AEROSPATIAL 2016”*  
26 - 27 October 2016, Bucharest, Romania, (held at INCAS, B-dul Iuliu Maniu 220, sector 6)  
Section 2 – Flight Mechanics and Systems Integration

**Abstract:** Parachute systems can be used to control the reentry trajectory of launcher upper stages, in order to lower the risks to the population or facilitate the retrieval of the stage. Several types of parachutes deployed at subsonic, supersonic and hypersonic speeds are analyzed, modeled as single and multistage systems. The performance of deceleration parachutes depends on their drag area and deployment conditions, while gliding parachutes are configured to achieve stable flight with a high glide ratio. Gliding parachutes can be autonomously guided to a low risk landing area. Sizing the canopy is shown to be an effective method to reduce parachute sensitivity to wind. The reentry trajectory of a launcher upper stage is simulated for each parachute system configuration and the results are compared to the nominal reentry case.

**Key Words:** parachute, systems, reentry, trajectory, launcher stage

## 1. INTRODUCTION

Some launcher upper stages with a trajectory that reaches above the Earth's atmosphere are expected to survive atmospheric reentry and reach the ground mostly intact [1]. For these stages there is interest in controlling the reentry phase using systems that can be added to the vehicle without extensive modifications or a large increase in mass. The main objective of the system is to modify the trajectory in order to move the ground impact point to a lower risk area relative to the nominal case. Changing the impact point is an effective method to reduce the reentry risks of launcher stages with non-demisable parts, if it is determined that the nominal case presents a high degree of risk to the population and property on the ground.

Parachutes are commonly used as aerodynamic decelerators and play an important role in the entry and descent of space vehicles. This type of devices serve multiple purposes which include vehicle deceleration from hypersonic to subsonic speeds, minimizing or providing a specific descent rate, or providing a steady descent trajectory. Parachute systems can have lower installation costs than other devices, since they do not require extensive modifications to the structure or large additional powered equipment. Parachutes also have a comparatively low weight, with the mass of a complete multistage system of about 120 kg.

This paper presents an analysis of the performance of three types of parachute systems for the control of the reentry phase, deployed at subsonic, supersonic and hypersonic speeds, modeled as single and multistage systems.

## 2. DECELERATION PARACHUTE SYSTEMS

The use of a deceleration parachute is a simple and cost effective method to reduce the speed and change the ground impact point of the stage during reentry. The efficiency of this approach depends on the parachute characteristics (drag area and deployment speed), but also on the payload mass and trajectory profile. Using a deceleration parachute will greatly increase the aerodynamic forces acting on the payload (the launcher stage), resulting in a shorter trajectory and moving the impact point uprange relative to the nominal case. This type of parachute can be used as a standalone system or in combination with a gliding parachute, which will be discussed in the following section.

The reentry trajectory analysis of the launcher stage with a deceleration parachute is based on a three degrees of freedom model, which describes the motion of the payload joined by a massless rigid link to a massless parachute, the link being pin-jointed at its attachment points to the payload. The axisymmetric deceleration parachutes are modeled by their drag force  $D_p$  and parachute oscillations about the direction of flow are considered negligible. Since the parachute mass is very small compared to its drag force, the tension force in the link to the payload can be approximated with  $D_p$  [2], [3], [4]. The external aerodynamic and gravitational forces acting on the launcher stage with a deceleration parachute, flying on a ballistic (non-lifting) trajectory are represented in Figure 1.

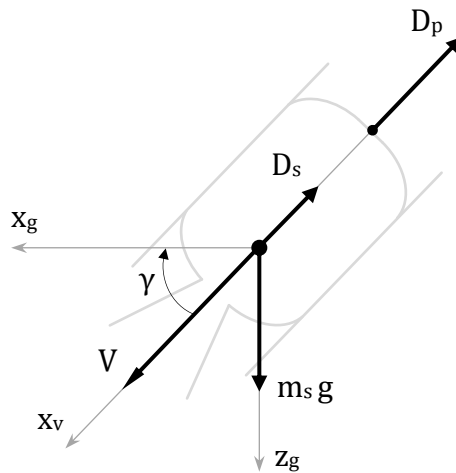


Figure 1 - Forces acting on the stage with deceleration parachute

Due to the low center of gravity of the launcher stage, the reentry occurs in a position with the engine nozzle in front, which can be considered as the zero angle of attack for reentry flight. The aerodynamic data for the reentering stage used in this paper correspond to Zefiro9, the third stage of the Vega launcher. The drag, lift and pitching moment coefficients were determined with a CFD analysis of the stage geometry, at Mach numbers from 0.3 to 5, and are in accordance with other CFD studies of the same vehicle for hypersonic speeds [5]. The stage is axially symmetric and an analysis of the moment as a function of attack angle

indicates two points of unstable equilibrium at  $0^\circ$  and  $180^\circ$  and two statically stable points at small positive and negative angles of attack. For the trajectory simulations in this paper, a ballistic reentry was assumed with the mean angle of attack of  $0^\circ$  and the drag coefficients corresponding to the position of stable equilibrium, as a function of Mach number.

The equations of translational motion for the launcher stage reentering Earth's atmosphere, rigidly linked to a deceleration parachute of negligible mass, expressed in the trajectory reference frame using spherical position and velocity components, in the case of a ballistic reentry without aerodynamic lift or side forces, can be written [6], [7], [8]:

$$\dot{V} = -\frac{D_p}{m_s} - \frac{D_s}{m_s} - g_r s \gamma - g_\delta c \gamma c \chi + \Omega^2 r c \delta (s \gamma c \delta - c \gamma s \delta c \chi) \quad (1)$$

$$V \dot{\gamma} = g_r c \gamma + g_\delta s \gamma c \chi + \Omega^2 r c \delta (c \gamma c \delta - s \gamma s \delta c \chi) + 2\Omega V c \delta s \chi + \frac{V^2}{r} c \gamma \quad (2)$$

$$V c \gamma \dot{\chi} = g_\delta s \chi + \Omega^2 r c \delta s \delta c \chi + 2\Omega V (c \gamma s \delta - s \gamma c \delta c \chi) + \frac{V^2}{r} c^2 \gamma t \delta s \chi \quad (3)$$

where  $D_s$  and  $D_p$  are the drag forces acting on the stage and the parachute;  $g_r$  and  $g_\delta$  are the radial and tangential components of the gravitational acceleration;  $m_s$  is the stage mass, which is assumed constant after parachute deployment;  $V$  is the stage speed with respect to the surface of the Earth;  $r$  is the distance from the center of the Earth to the CoG of the stage;  $\gamma$  is the flightpath angle between  $V$  and the local horizontal plane, which is negative when  $V$  is oriented below the local horizon;  $\chi$  is the heading angle which defines the projection of  $V$  in the local horizontal plane with respect to the local north, which is positive to the east;  $\Omega$  is the rotational rate of the Earth and  $\delta$  is the local latitude; the sine, cosine and tangent functions have been abbreviated with  $s$ ,  $c$  and  $t$ .

For the simulation of the stage reentry with a large supersonic deceleration parachute a model of the Viking Lander parachute was used. This parachute has been extensively tested in three Mach regimes (subsonic, transonic and supersonic), both in the wind tunnel and with multiple airdrops, and it has been found to meet all requirements for planetary reentry. The nominal diameter of the parachute is  $D_p = 16.15$  m, with a reference area of  $S_p = (\pi/4)D_p^2 = 204.96$  m<sup>2</sup> and the mass of the parachute is  $m_p = 44$  kg. The parachute was tested at a maximum deployment speed of Mach 2.2 and an altitude of 43 km. Figure 2 (left) shows the variation of the Viking parachute drag coefficient with Mach number [9], which represents an average of measurements from flight data, in the wake of a blunt forebody.

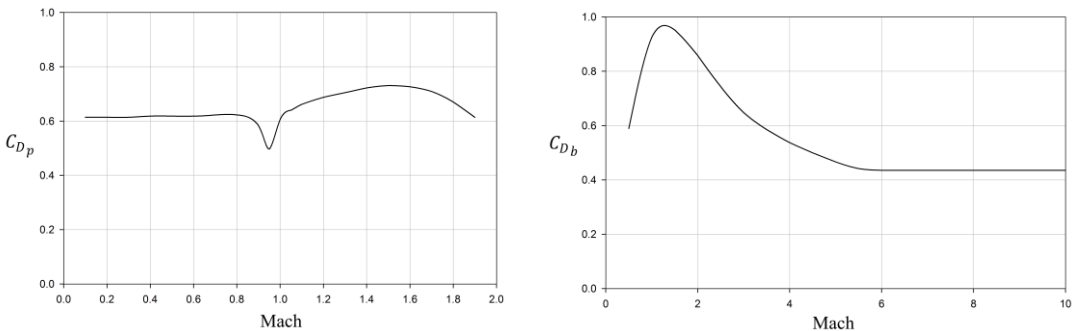


Figure 2 - Viking parachute (left) and ballute (right) drag coefficient with Mach number

The simulation of the reentry with a hypersonic trailing isotenoid decelerator, also known as a ballute, used a model of a ballute which was developed by the Goodyear Aerospace Corporation for the ADDPEP Program, which has been successfully tested in the wind tunnel and in airdrops, at speeds of up to Mach 10 and altitudes up to 64 km. The shape and structure of the ballute are based on multiple requirements, which include obtaining a positive and nearly uniform stress structure (isotenoid), increasing the aerodynamic stability of the payload and minimizing weight. The nominal diameter of the ballute is  $D_b = 1.52$  m, with the reference area taken as the projected area,  $S_b = (\pi/4)D_b^2 = 1.814$  m<sup>2</sup>, and the total mass of the ballute is  $m_b = 9$  kg. Figure 2 (right) shows the variation of the ballute drag coefficient with Mach number [10], [11], which represents an average of measurements from multiple sources, in the wake of a blunt forebody.

### 3. GLIDING PARACHUTE SYSTEMS

A more effective and versatile approach to controlling the reentry trajectory of the stage is to use a gliding parachute, also known as a ram-air parachute. The development of ram-air parachutes has seen significant technological advancements in recent years, with payload capacities of up to 19.000 kg being successfully tested [12], which makes feasible the controlled descent and even recovery of launcher stages with a single parachute. For the control of the reentry phase, a gliding parachute is used to achieve a longer steady gliding flight, which will move the impact point further downrange. Ram-air parachutes can also be fitted with guidance and control systems, enabling them to have more control over the impact point location by steering to a lower risk landing area. Achieving a longer horizontal range depends on deploying the gliding parachute at higher altitudes and configuring the system to fly at a high  $L/D$  ratio (glide ratio).

Since the maximum deployment speed of ram-air parachutes is relatively low, around 150 knots or 77 m/s, for reentry where the initial speeds are high, the range of this type of parachute is greatly increased when used as a second stage in conjunction with a deceleration parachute such as those presented in section 2. In this case the deceleration parachutes are deployed first in order to lower the system speed, then once the speed has dropped below the required value the deceleration parachute is released and the gliding parachute is deployed.

The analysis of the gliding parachute system is based on a three degrees of freedom model, which describes the translational and rotational motion of the parachute joined by a rigid link to the payload. Gliding is a steady state flight which, if the system is flying in still air (without winds), results in a steady descent with a total speed  $V$  and a glide (flightpath) angle  $\gamma$ . The forces acting on the system in steady gliding flight can be expressed in a horizontal reference frame [2], [13], [14]:

$$(L_c + L_l + L_s) \sin \gamma - (D_c + D_l + D_s) \cos \gamma = 0 \quad (4)$$

$$(m_s + m_c)g - (L_c + L_l + L_s) \cos \gamma - (D_c + D_l + D_s) \sin \gamma = 0 \quad (5)$$

where  $L_c + L_l + L_s = L$  is the total lift force and  $D_c + D_l + D_s = D$  is the total drag force of the system, with subscripts  $c$ ,  $l$  and  $s$  denoting forces acting on the canopy, suspension lines and payload (stage);  $m_s + m_c = M$  is the total system mass, with  $m_s$  and  $m_c$  being the masses of the payload and canopy. For steady gliding flight the resultant aerodynamic force of the system is oriented vertically,  $F = \sqrt{L^2 + D^2} = L \cos \gamma + D \sin \gamma$ . Figure 3 shows the forces and moments acting on the parachute system.

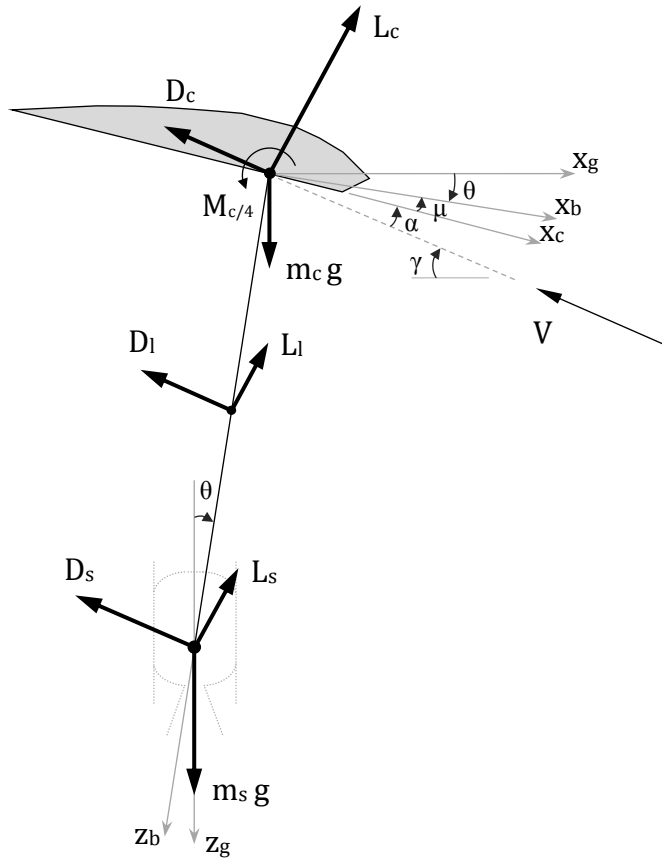


Figure 3 - Forces and moments acting on the stage with gliding parachute

In Figure 3  $x_g$  and  $z_g$  are the horizontal and vertical axes, with  $z_g$  oriented along the local vertical;  $x_b$  and  $z_b$  are the payload axes, with  $z_b$  oriented from the canopy CoG to the payload; and  $x_c$  is the canopy axis which defines the attitude of the canopy relative to the airspeed.

The glide angle of the parachute system can be expressed from equation (4)

$$\frac{1}{\tan \gamma} = \frac{L}{D} = \frac{C_L}{C_D} \tag{6}$$

where  $C_L$  and  $C_D$  are the total lift and drag coefficients of the system. The airspeed of the system in steady gliding flight results from equation (5)

$$V = \left[ \frac{2 \cdot Mg}{\rho \cdot S_p} \cdot \frac{1}{(C_L^2 + C_D^2)^{0.5}} \right]^{0.5} \tag{7}$$

The horizontal and vertical components of the airspeed have the expression

$$u = V \cos \gamma \qquad w = V \sin \gamma \tag{8}$$

The horizontal range of the system in still air can be expressed in relation to the deployment altitude of the parachute  $H_d$

$$R_h = H_d / \tan \gamma \tag{9}$$

Equation (6) shows that in still air, the glide angle and the horizontal range of the parachute system for a given altitude loss are a function only of the system glide ratio  $L/D$ , while equation (7) indicates that the speed depends on system mass, canopy area, altitude, as well as the aerodynamic characteristics of the system.

Figure 4 shows the lift, drag and pitching moment coefficients of a ram-air canopy with an aspect ratio of  $A = 2.5$  and  $S_p = 300 \text{ m}^2$  [14], for angles of attack of  $\alpha = 0^\circ \dots 10^\circ$ .

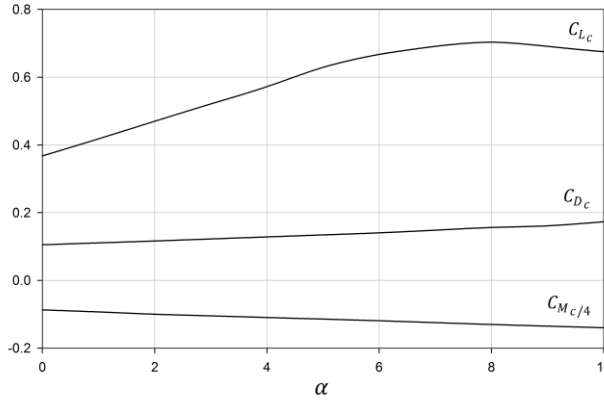


Figure 4 - Lift, drag and pitching moment coefficients of a ram-air canopy

Assuming the parachute system is rigid and that the canopy CoG is located at the quarter chord point, the total pitching moment coefficient of the system about the quarter chord point of the canopy, as shown in Figure 3, can be expressed [14], [15]:

$$C_M = C_{M_{c/4}} + \frac{R}{c} \left[ \left( C_{L_s} + \frac{1}{2} C_{L_l} \right) \sin(\alpha + \mu) - \left( C_{D_s} + \frac{1}{2} C_{D_l} \right) \cos(\alpha + \mu) \right] + C_{M_g} \quad (10)$$

where  $C_{M_{c/4}}$  is the aerodynamic pitching moment coefficient of the canopy about the quarter chord point;  $C_{L_s}$  and  $C_{D_s}$  are the stage lift and drag coefficients expressed using the reference area of the canopy,  $S_p$ ;  $C_{L_l}$  and  $C_{D_l}$  are the lift and drag coefficients of the parachute lines,  $C_{D_l} = [ndR \cos^3(\alpha + \mu)]/S_p$  and  $C_{L_l} = [ndR \cos^2(\alpha + \mu) \sin(\alpha + \mu)]/S_p$ , expressed in terms of the number of lines,  $n$ , and line diameter,  $d$ ;  $R$  is the distance from the quarter chord point to the payload, along the  $z_b$  axis;  $c$  is the wing chord and  $b$  is the wing span;  $\mu$  is the canopy rigging angle between the payload and canopy axes;  $C_{M_g}$  is the moment coefficient of the payload weight about the quarter chord point,  $C_{M_g} = (m_s g R \sin \theta) / 0.5 \rho V^2 S_p c$ ; and  $\theta$  is the pitch angle between the payload and horizontal axes, so that

$$\theta = \gamma - \alpha - \mu \quad (11)$$

For the analysis of the system configuration, both the glide and pitch angles have been chosen positive below the horizon (see Figure 3), with the payload weight  $m_s g$  generating a positive pitching moment about the quarter chord point for a positive pitch angle.

#### 4. GLIDING PARACHUTE PERFORMANCE

The gliding parachute system can be configured to fly at a high  $L/D$  ratio by rigging the canopy, i.e. by positioning the payload such that the equilibrium attitude of the system is at the desired angle of attack. The parachute is in stable equilibrium when the sum of all

pitching moments is zero ( $C_M = 0$ ) and the slope of the pitching moment curve is negative ( $dC_M/d\alpha < 0$ ). Using pitching moment data for the canopy presented in Figure 4 and solving equation (10) for the system parameters  $R/b = 0.6$ ,  $m_s = 1383$  kg,  $m_c = 60$  kg,  $n = 270$ ,  $d = 25$  mm,  $C_{D_s} = 0.03$  and  $C_{L_s} = 0$ , the total pitching moment coefficient of the system was calculated as a function of the angle of attack, for  $\mu = 1^\circ \dots 10^\circ$ . Values for which  $C_M = 0$  define configurations in which the system achieves stable gliding flight. The variation of the system  $L/D$  ratio with the angle of attack is calculated for the most useful rigging angles of  $\mu = 1^\circ \dots 5^\circ$ . Figure 5 presents the variation of the moment coefficient  $C_M$  (left scale) and the  $L/D$  ratio of the system (right scale), with the attack and rigging angles.

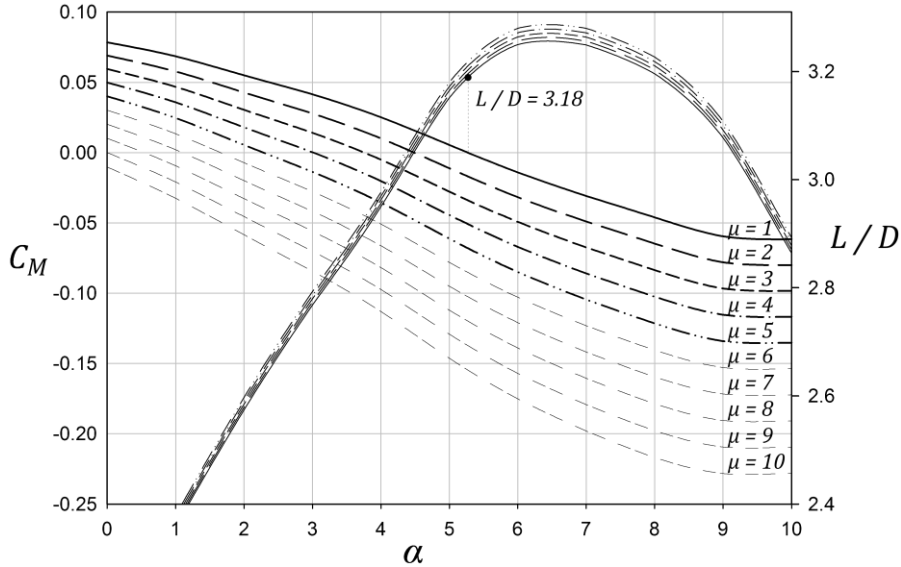


Figure 5 - Variation of  $C_M$  (left scale) and  $L/D$  (right scale) with the attack and rigging angles

An analysis of the possible  $L/D$  ratios in Figure 5 at equilibrium configurations indicates that good performances can be obtained by rigging the parachute with  $\mu = 1^\circ$ . In this case, the parachute will fly at an angle of attack of  $\alpha = 5.25^\circ$  resulting in an  $L/D$  ratio of 3.18, with a speed of  $V_0 = 10.69$  m/s at sea level. The total lift and drag coefficients of the system in this configuration are  $C_L = 0.642$  and  $C_D = 0.202$ , calculated using the reference area of the canopy  $S_p = 300$  m<sup>2</sup>.

Ram-air parachutes can be fitted with automatic guidance and control systems and used as autonomous precision aerial delivery systems (PADS). PADS have the capability to change course by executing turn maneuvers with achievable turn rates of up to  $10^\circ/s$ , making them a good solution to control the trajectory during the final subsonic flight phase by maintaining a course to a low risk landing area. Since the turn radius is small, assuming no wind the system can deliver the payload anywhere in a circular area centered on the point of deployment, with the maximum horizontal range (maneuvering radius)  $R_h$  from the center.

During practical missions however there is usually some wind present in the area where the parachute is flying. Some areas have prevailing wind directions which may be taken into account in the mission planning stage. If the mission has a desired landing area for the stage situated along a course  $\psi_c$  relative to the current position, then assuming a horizontal wind with speed  $u_w$  and direction  $\psi_w$  measured from the north, the guided parachute system can maneuver and fly on a heading with a wind correction angle  $\varepsilon$  which will compensate the

deviation from the course  $\psi_c$  caused by the wind. The speed of the system flying on a desired course against the wind is presented in Figure 6.

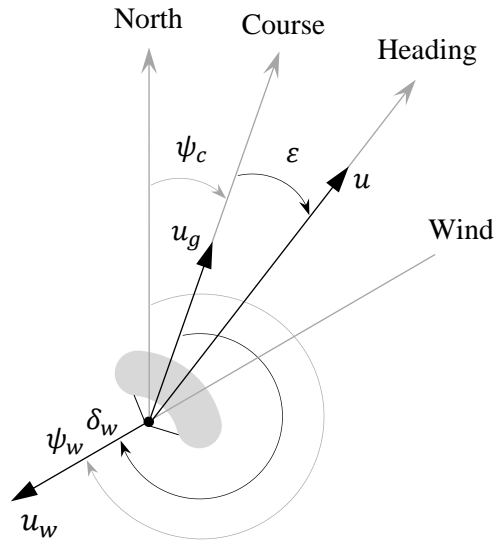


Figure 6 - Speed of the parachute system

The horizontal groundspeed of the system is given by the vector addition of the airspeed and wind speed (wind triangle),  $\mathbf{u}_g = \mathbf{u} + \mathbf{u}_w$ . The course remains constant if the groundspeed component normal to the course  $\psi_c$  is zero,  $u_{g\perp} = u \sin \varepsilon + u_w \sin(\delta_w) = 0$ , where  $\delta_w = \psi_w - \psi_c$ . The wind correction angle, which can be calculated using sensor data and programmed into an onboard guidance computer, can be expressed

$$\varepsilon = \arcsin \left[ -\frac{u_w}{u} \sin(\delta_w) \right] \quad (12)$$

The resulting horizontal groundspeed of the parachute system is oriented along  $\psi_c$ ,  $u_g = u \cos \varepsilon + u_w \cos \delta_w$ . For the system to be able to fly on the desired course  $\psi_c$  at all altitudes against a wind with the speed  $u_w$  and direction  $\delta_w$ , the system's horizontal airspeed must be higher than the speed of the wind along  $\psi_c$  at sea level

$$u_0 \cos \varepsilon_0 > -u_w \cos \delta_w \quad (13)$$

In the most unfavorable case of flying into a headwind ( $\delta_w = 180^\circ$ ) with the speed  $u_w$ , the horizontal groundspeed of the parachute system becomes  $u_g = u - u_w$ . The condition to be able to fly against the headwind at all altitudes is for the system's horizontal airspeed to be higher than the speed of the wind, in which case relation (13) reduces to

$$u_0 > u_w \quad (14)$$

The sensitivity of the ram-air parachute performance to wind can be reduced by an appropriate sizing of the canopy, since gliding speed is inversely proportional to the square root of the canopy area, as indicated in equation (7). Ideally the wing loading of the parachute is chosen high enough that the system has some margin over possible winds, but not to the point where deformation of the wing becomes significant. Assuming the parachute system can be rigged to fly with approximately the same  $C_L$  and  $C_D$  coefficients calculated in

section 3 for all canopy sizes, Figure 7 shows the system horizontal airspeed in stable gliding flight at sea level,  $u_0$ , as a function of canopy area and total system mass.

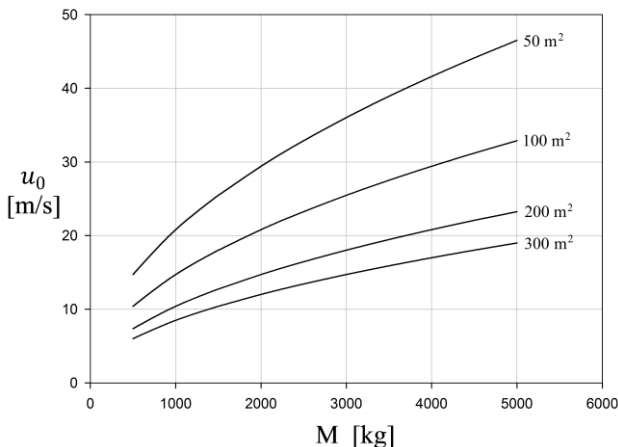


Figure 7 - Variation of horizontal airspeed with canopy area and system mass

A more general analysis of canopy sizing can be done by expressing  $u_0$  as a function of wing loading. Figure 8 shows the variation of  $u_0$  with wing loading, for different  $L/D$  ratios and a total lift coefficient  $C_L$  of 0.6 and 0.7 for the parachute system.

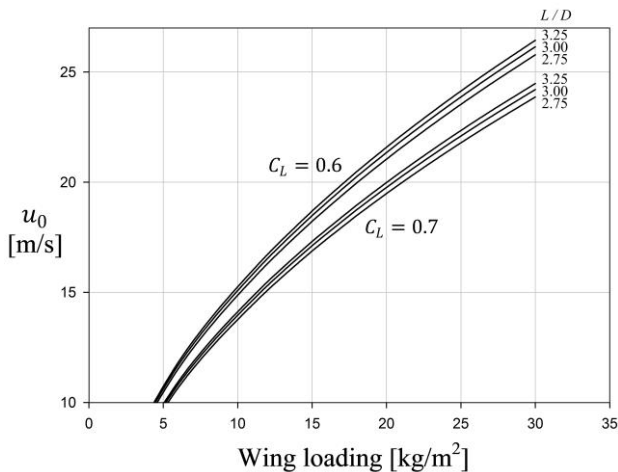


Figure 8 - Variation of horizontal airspeed with wing loading and  $L/D$  ratio

### 5. NUMERICAL SIMULATIONS

The performance of the parachute systems described in the previous sections was evaluated by numerical simulations of the reentry trajectory of the Zefiro9 launcher stage. In order to show the effectiveness of each type of device in changing the impact point of the stage, four cases were considered with different system configurations, consisting of 1 to 3 stage systems. Each simulation is compared to the nominal reentry case, which represents the original trajectory of the stage, without any parachute systems. All trajectory simulations were performed with the Astos Trajectory Optimization Software, used by the European Space Agency for launch and reentry vehicle trajectory simulation and optimization [16].

The first system configuration consists of the Viking supersonic deceleration parachute (DP), with a deceleration flight phase from deployment at Mach 2.2 until impact. The second configuration represents a 2-stage system which includes the hypersonic textile ballute (TB) and the DP, with two deceleration phases starting with the deployment of each device at Mach 10 and Mach 2.2, respectively. The third configuration represents a 2-stage system which includes the DP and the subsonic ram-air parachute (RAM), with a deceleration phase starting at Mach 2.2 and a gliding phase which starts with the deployment of the RAM at the speed of 77 m/s. The fourth configuration consists of a 3-stage system which includes the TB, DP and RAM, with two deceleration phases and one final gliding phase. Table 1 lists the total mass of the system, the deployment altitudes for each parachute and the change of impact point relative to the nominal case (without parachutes), for each configuration.

Table 1 - Parachute system configuration and performance

System configuration	Mass	Deployment altitude (km)			Impact point
		TB	DP	RAM	
1 stage DP	44 kg	–	23.5	–	- 6 km
2 stage TB + DP	53 kg	36.1	24.6	–	- 7 km
2 stage DP + RAM	104 kg	–	22.9	22.5	+ 76 km
3 stage TB + DP + RAM	113 kg	35.8	24.3	23.8	+ 75 km

The simulation results show that the RAM parachute is effective at moving the impact point over significant distances, provided that it is deployed at high altitudes. The DP is very efficient in reducing the speed of the stage, reaching 77 m/s in just six seconds after it is deployed, thus greatly increasing the range of the RAM. The hypersonic TB is inefficient in changing the impact point for this type of payload and trajectory profile, because of its small drag area. The impact point changes for cases 2 and 4, with configurations including the TB, have very small differences to cases 1 and 3 respectively, which have similar configurations but without the TB. Figures 9 and 10 show the system altitude and speed variation with time in cases 1 and 3, from the reentry altitude of 100 km. The solid line represents the current case and the dashed line shows the nominal case trajectory.

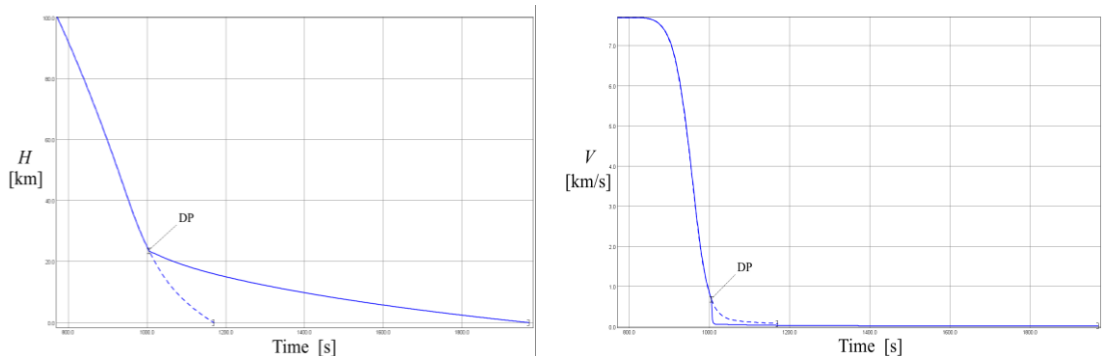


Figure 9 - Altitude (left) and speed (right) variation with time for case 1

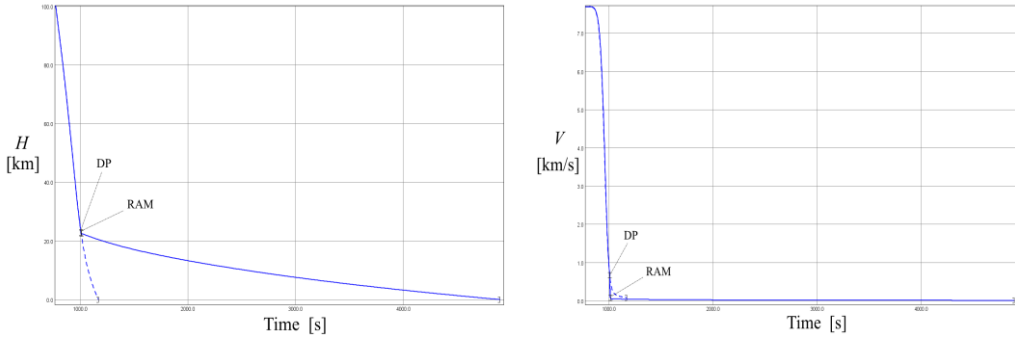


Figure 10 - Altitude (left) and speed (right) variation with time for case 3

The performance of the gliding ram-air parachute entails further consideration, since initial sizing of the canopy determines the range of the system in the presence of wind. In order to evaluate the influence of wind on the performance of the gliding parachute presented in section 3, the trajectory of the system in case 3 was simulated with headwinds of 5, 7 and 9 m/s. The range of the system in each scenario is compared to the original case without wind, to show the sensitivity to wind for a given canopy size and wing loading.

To assess the effectiveness of reducing the sensitivity to wind of the parachute by sizing the canopy, the trajectory of the system in case 3 was also simulated for a canopy area of 100 m<sup>2</sup>, with headwinds of 5, 7 and 9 m/s. Table 2 shows the system parameters, wind speed and the range of the parachute system in case 3 for each scenario.

Table 2 - Ram-air parachute sensitivity to headwind

Canopy area	System $L/D$	Total mass	Wing loading	Wind speed	System range
300 m <sup>2</sup>	3.18	1443 kg	4.8 kg/m <sup>2</sup>	0 m/s	71.35 km
300 m <sup>2</sup>	3.18	1443 kg	4.8 kg/m <sup>2</sup>	5 m/s	73 %
300 m <sup>2</sup>	3.18	1443 kg	4.8 kg/m <sup>2</sup>	7 m/s	62 %
300 m <sup>2</sup>	3.18	1443 kg	4.8 kg/m <sup>2</sup>	9 m/s	51 %
100 m <sup>2</sup>	3.18	1423 kg	14.2 kg/m <sup>2</sup>	5 m/s	82 %
100 m <sup>2</sup>	3.18	1423 kg	14.2 kg/m <sup>2</sup>	7 m/s	76 %
100 m <sup>2</sup>	3.18	1423 kg	14.2 kg/m <sup>2</sup>	9 m/s	70 %

The simulation results show that wind can have a significant influence on the system range, with a decrease in performance as low as 51% for a parachute with low wing loading in case of a moderate headwind. The simulations with the second canopy show that proper sizing of the canopy relative to the payload weight is an effective method to reduce the wind sensitivity of the ram-air parachute. A wing loading of the parachute of 14.2 kg/m<sup>2</sup> results in a system range of 50.1 km for the highest moderate headwind of 9 m/s, which represents a performance of 70% compared to the scenario without wind, indicating that wing loadings of 15 kg/m<sup>2</sup> or higher ensure a margin over low to moderate wind speeds.

## 6. CONCLUSIONS

Parachute systems are effective at controlling the reentry trajectory of launcher upper stages, assuming proper sizing and configuration of the system for the mission requirements.

The large supersonic parachute is very efficient in rapidly decelerating the stage, but less efficient in changing the impact point as a standalone system, because of its comparatively low deployment speed. Due to its small drag area, the hypersonic ballute is inefficient in changing the impact point for this type of payload and trajectory profile.

The subsonic gliding parachute is effective at moving the impact point over large distances, when configured to fly at high glide ratios and deployed at high altitudes. For the large initial speeds characteristic of atmospheric reentry, the efficiency of the gliding parachute is greatly increased in a multistage system which ensures deceleration at higher altitudes and extends its flight range.

Gliding parachutes can be autonomously guided to a low risk landing area. Wind speed has a significant influence on the range of the parachute system. Sizing the canopy is an effective method to reduce parachute sensitivity to wind, with wing loadings of 15 kg/m<sup>2</sup> or higher giving a margin over low to moderate wind speeds.

## ACKNOWLEDGEMENT

The work presented here was performed partly under the *Deorbitation Design for Demise* project, contract no. 400109249/13/JLV, for the European Space Agency *Launcher Upper Stages Technology Development for Future Launchers Preparatory Program*.

## REFERENCES

- [1] D. Koppenwallner, *Zefiro9 Stage Re-entry Analysis Documentation*, HTG Vega Memo 3-12 -07, 2008.
- [2] D. J. Cockrell, *The aerodynamics of parachutes*, AGARD-AG-295, 1987.
- [3] M. Sudars and A. Saluzzi, Modeling Of Parachute Dynamics in a Synthetic Flight Mechanics Simulations' Environment, *AIAA Paper 2009-2943*.
- [4] K. F. Doher, *Parachute Flight Dynamics and Trajectory Simulation*, Heinrich Parachute Systems Short Course, University of St. Louis, 2002.
- [5] F. Stella and M. Giangi, *Numerical Study of VEGA third stage re-entry phase and cross-check of HTG SCARAB analysis*, Vega Programme Report, 2009.
- [6] C. Wieland, *Computational Space Flight Mechanics*, Springer, 2010.
- [7] A. Tewari, *Atmospheric and Space Flight Dynamics*, Birkhäuser, 2007.
- [8] E. Mooij, *The motion of a vehicle in a planetary atmosphere*, Delft University Report LR-768, 1994.
- [9] R. J. Bendura, R. R. Lundstvom, P. G. Renfroe, S. R. LeCroy, *Flight tests of Viking parachute system in three Mach number regimes*, NASA TN D-7734, 1974.
- [10] F. Bloetscher, *The Aerodynamic Deployable Decelerator Performance-Evaluation Program (ADDPEP)*, Phase II, Technical Report AFFDL-TR-67-25, 1967.
- [11] B. P. Smith, C. L. Tanner, M. Mahzari, I. G. Clark, R. D. Braun, F. M. Cheatwood, A Historical Review of Inflatable Aerodynamic Decelerator Technology Development, *IEEEAC paper 1276, Version 3*, 2010.
- [12] J. C. Berland, J. Barber, B. Gargano, B. P. Bagdonovich, Autonomous Precision Delivery of 42,000 Pounds (19,000 kg) Under One Parachute, *AIAA Paper 2009-2928*.
- [13] T. W. Knacke, *Parachute Recovery Systems Design Manual*, NWC TP6575, Para Publishing, 1991.
- [14] J. S. Lingard, *Precision aerial delivery seminar, Ram-air parachute design*, 13<sup>th</sup> AIAA Aerodynamic Decelerator Systems Technology Conference, 1995.
- [15] J. S. Lingard, The Aerodynamics of Gliding Parachutes, *AIAA-86-2427-CP*, 1986.
- [16] G. Ortega, A. Blasco, S. Weikert, *Space safety trajectory optimization and debris analysis using ASTOS at ESA*, 37<sup>th</sup> COSPAR Scientific Assembly. Montréal, Canada, p.2300, 13–20 July 2008.